LANGMUIR Article
Cite This: Langmuir 2017, 33, 14340−14346
pubs.acs.org/Langmuir

Dissolution and Characterization of Boron Nitride Nanotubes in Superacid

Olga Kleinerman,[†] Mohammed Adnan,[‡] Daniel M. Marincel,[‡] Anson W. K. Ma,[‡,⊥] E. Amram Bengio,[†,‡] Cheol Park,[§] Sang-Hyon Chu,[∥] Matteo Pasquali,*[,‡] and Yeshayahu Talmon*[,†]

[†]Department of Chemical Engineering, Technion-Israel Institute of Technology and the Russell Berrie Nanotechnology Institute (RBNI), Haifa 3200003, Israel

[‡]Department of Chemical and Biomolecular Engineering and Department of Chemistry, The Smalley-Curl Institute, Rice University, Houston, Texas 77005, United States

[§]Advanced Materials and Processing Branch, NASA Langley Research Center, Hampton, Virginia 23681, United States

[∥]National Institute of Aerospace, 100 Exploration Way, Hampton, Virginia 23666, United States

Supporting Information

ABSTRACT: Boron nitride nanotubes (BNNTs) are of interest for their unique combination of high tensile strength, high electrical resistivity, high neutron cross section, and low reactivity. The fastest route to employing these properties in composites and macroscopic articles is through solution processing. However, dispersing BNNTs without functionalization or use of a surfactant is challenging. We show here by cryogenic transmission electron microscopy that BNNTs spontaneously dissolve in chlorosulfonic acid as disentangled individual molecules. Electron energy loss spectroscopy of BNNTs dried from the solution confirms preservation of the sp^2 hybridization for boron and nitrogen, eliminating the possibility of BNNT functionalization or damage. The length and diameter of the BNNTs was statistically calculated to be ∼4.5 μm and ∼4 nm, respectively. Interestingly, bent or otherwise damaged BNNTs are filled by chlorosulfonic acid. Additionally, nanometer-sized synthesis byproducts, including boron nitride clusters, isolated single and multilayer hexagonal boron nitride, and boron particles, were identified. Dissolution in superacid provides a route for solution processing BNNTs without altering their chemical structure.

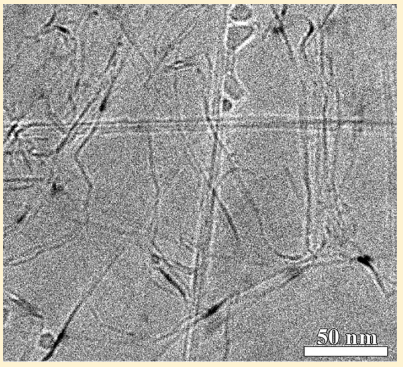

INTRODUCTION

Boron nitride nanotubes (BNNTs) are synthetic inorganic allotropes of hexagonal boron nitride (h-BN); they have been under intense study since their first synthesis in 1995.[1] BNNTs combine excellent mechanical properties[2−6] with low density, superior thermochemical stability,[7,8] electrical insulation independent of chirality,[9,10] and interesting optical properties.[11,12] BNNTs also exhibit intrinsic piezoelectricity[13,14] and neutron radiation shielding capability.[15] As such, BNNTs have great potential to serve as building blocks for many novel nanoscale devices[16−24] or as a part of new generation composite materials.[25−27]

In many ways, the current state of BNNT studies is reminiscent of the early stages of carbon nanotube (CNT) research, with focus on synthesis routes and theoretical research.[3] To this date, there are about 10 BNNT manufacturers worldwide providing gram-scale quantities for research purposes. These are primarily focused on using BNNTs as a filler material for composites.[25,28,29] Regardless of production method, BNNTs suffer from poor solubility in common solvents[30−38] much like other nanoscale materials such as CNTs, other inorganic nanotubes, and graphene. Our study focuses on a wet processing technique for which stable solutions serve as the starting point for macroscopic films, membranes, and fibers.

Chlorosulfonic acid (CSA) has been shown to be a true thermodynamic solvent for single- and multiwalled CNTs as well as graphene; strong acids reversibly protonate the carbon surface,[39−42] which provides a mechanism for countering the strong van der Waals attraction between nanoscale carbon structures. Here, we mix BNNTs with superacids and study their dissolution via the cryogenic-temperature transmission electron microscopy (cryo-TEM) methodology that we had previously developed for highly acidic systems.[43] Direct imaging of the BNNT/CSA mixtures in their native state shows that in CSA, BNNTs are individually dispersed on the molecular level. While the superacid−BNNT interaction is not well understood, we hypothesize that CSA protonates the more electronegative nitrogen atoms, as was previously reported for h-BN in CSA.[44] The protonation causes BNNTs to accrue a net positive charge, resulting in intertube repulsion and spontaneous dissolution in superacids. Along with the observation of

Received: October 4, 2017
Revised: November 20, 2017
Published: November 22, 2017

DOI: 10.1021/acs.langmuir.7b03461
Langmuir 2017, 33, 14340−14346

individual BNNTs dissolution, we also identify impurities in the BNNT material; the presence of these impurities limits the quality of BNNT liquid phases. By combining several techniques, we estimate BNNT length, study BNNT structural defects, and characterize the entire population of synthesis-related impurities, providing key input for future postprocessing and manufacturing methods.

EXPERIMENTAL SECTION

We studied long BNNTs produced by a novel high temperature–pressure (HTP) method at the National Institute of Aerospace/NASA Langley Research Center (Hampton, VA). The synthesis involves forced condensation of BNNTs in an ascending plume of pure boron vapor at elevated pressure in a nitrogen chamber.[45] Pure (99.9%) chlorosulfonic acid (CSA) was used as received from Sigma-Aldrich. The chemicals were stored in a glovebox under continuous flow of dry air.

We mixed the BNNT material with CSA at an initial concentration of 100 ppm inside a glovebox, continuously purged with dry air. The BNNT/CSA mixture, sealed with Teflon tape in a vial, was subjected to stir-bar mixing for 24–48 h. Cryo-TEM specimens of BNNT/CSA solutions were prepared following the methodology developed for direct imaging of CNTs in superacid solutions.[43,46] In brief, a drop of the solution, about 3 μL, was applied to a perforated carbon film (PCF) supported on a copper TEM grid (Ted Pella, Redding, CA), held by tweezers inside a controlled environment vitrification system (CEVS),[47] enclosed within a flexible polyethylene "glovebag" (Sigma-Aldrich). Before use, the PCFs were cleaned with glow-discharge air-plasma (Pelco easiGlow, Ted Pella Inc., Redding, CA), for better wettability of the support film. The CEVS, kept at 25 °C, was continuously purged with pure dry nitrogen gas, preventing any moisture from accumulating in the system. Because CSA interacts with cellulose, we used glass-fiber filter paper (instead of cellulose filter-paper) to blot the liquid drops into thin films. We plunged the liquid specimen into boiling liquid nitrogen to vitrify the specimen. While boiling liquid nitrogen gives much slower cooling rates than liquid ethane at its freezing point,[48] it does vitrify CSA, but does not interact with it. The speed of sample preparation plays an important role; the entire specimen preparation procedure takes just a few seconds to prevent the reaction of CSA with the copper grid.

Cryo-TEM imaging was performed with either a Philips CM120 or an FEI Tecnai T12 G^2 TEM, equipped with a LaB_6 electron gun, and operated at an accelerating voltage of 120 kV. Specimens were equilibrated in the microscope below −178 °C in an Oxford CT-3500 cryo-holder (Philips) or a Gatan 626 (FEI) cryo-holder. Cryo-specimens were examined using the low-dose imaging mode to minimize electron-beam radiation-damage. Images were recorded digitally by a Gatan Multiscan 791 cooled CCD camera (on the CM 120) or a Gatan US1000 CCD camera (on the T12), using the Digital Micrograph software.

Statistical analysis on the BNNT length from cryo-TEM was conducted using the bootstrap method previously reported.[49] Thirty-three cryo-TEM images were used for the analysis, with resulting error of ±0.66 μm, or 15% of the average BNNT length. To understand the correlation between the physical BNNT characteristics, such as aspect ratio, defects and impurities, and their interactions with superacid, we continued to characterize *the same BNNTs*, after performing cryo-TEM. For that purpose, cryo-TEM grids are removed from the electron microscope, dipped in water to remove the acid and its residues, and then dried overnight under vacuum. In this manner, the thin (up to 20 nm thick) BNNT film is left on the TEM grid for further characterization of BNNTs by room-temperature HR-TEM and HR-SEM. To determine the distribution of BNNT diameter and number of walls, dried cryo-TEM grid specimens were analyzed by high-resolution TEMs: a monochromated FEI Titan 80-300 S/TEM (FEI, Eindhoven, The Netherlands), equipped with a C_s corrector operated at 80 kV acceleration voltage, and a FEI Talos 200C TEM (FEI, Eindhoven, The Netherlands) operated at 200 kV, and equipped with Ceta 16 M high speed CMOS camera. Due to TEM imaging in underfocus mode and Photoshop ruler tool inaccuracy, we estimate a ± 5% error in diameter measurements. High-resolution SEM images were taken on Zeiss Ultra Plus SEM at very low electron acceleration voltage (0.7–2 kV) and short working distance (2.9–3.3 mm). Both the in-the column ("InLens") and the Everhart-Thornley ("SE2") secondary electron imaging detectors were used in this study. To improve BNNT conductivity during imaging, we used double-side copper tape to attach BNNTs to the specimen holder. To identify fine chemical structure of observed features, EELS spectra were acquired in scanning-transmission (STEM) mode on the Titan by using high angle angular dark field (HAADF) and post column Gatan (Pleasanton, CA) Tridiem 866 EELS detectors. Energy filtered images were collected with a Gatan GIF system on a Philips CM200, with a LaB_6 emitter, operated at 200 kV, while elemental maps were obtained using a standard three-window technique that assumed an Ae^{-r} model for the background.[50] For elemental maps the window included the K-absorption edge, and background subtractions were based on curve fitting from two pre-edge maps and one postedge map for each element.

RESULTS AND DISCUSSION

Immediately upon contact with CSA, the BNNT material forms small aggregates (Figure 1; left). Within 24 h of gentle stir-bar mixing, the liquid turns golden yellow, although small gray agglomerates are still visible to the naked eye, as shown in Figure 1 (right).

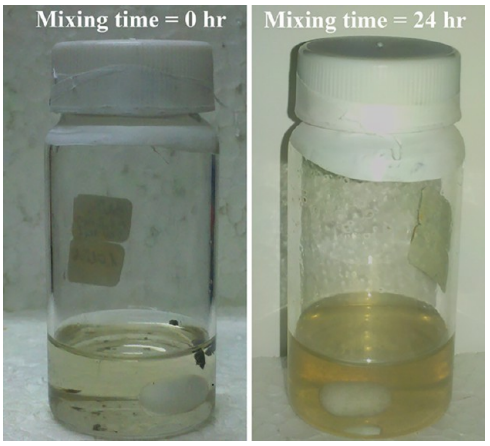

Figure 1. BNNT solution in CSA upon CSA addition and after 24 h of stir-bar mixing.

In fact typical cryo-TEM images reveal individualized BNNTs in CSA (Figure 2). The BNNTs appear as darker threads in the CSA matrix (white arrows). This is the first direct evidence of CSA dissolving BNNTs by overcoming the intertube attractions. HR-TEM of dry BNNT grids (see the Supporting Information) shows mostly double-walled BNNTs with a small fraction of single-walled and multiwalled BNNTs, with a mean diameter of 3.8 ± 0.2 nm (see the Supporting Information). The observed number of walls is consistent with the individual BNNT statistics reported previously, while the average diameter observed here is significantly higher than previously reported.[14] We use cryo-TEM images of individual BNNTs in CSA to estimate the BNNT length, based on statistical image analysis. Using the bootstrap method,[49] we measure an average BNNT length of 4.53 ± 0.66 μm (see the Supporting Information), 2 orders of magnitude lower than previously estimated via statistical analysis of SEM images of as-grown, bundled BNNTs.[45]

DOI: 10.1021/acs.langmuir.7b03461
Langmuir 2017, 33, 14340–14346

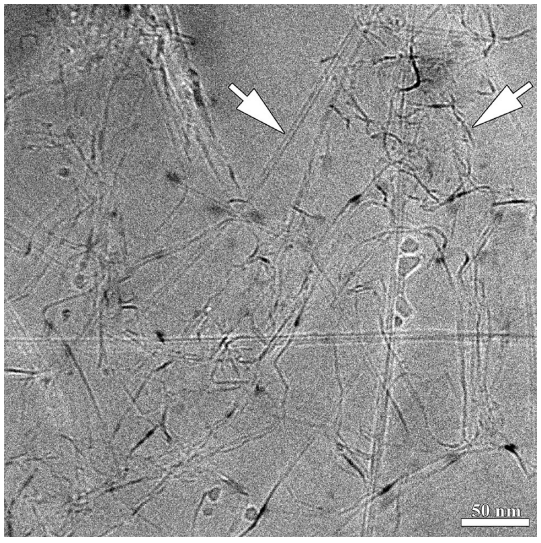

Figure 2. Cryo-TEM image of individualized BNNTs in CSA. The BNNTs appear as darker threads in the CSA matrix (white arrows).

BNNTs were found to be more stable under the electron beam relative to CNTs and graphene in similar conditions[43] with negligible electron-beam radiation damages observable at the BNNT/CSA interface despite relatively long exposure to the e-beam (about 50 e/Å^2).

EELS analysis (see the Supporting Information) was conducted on TEM grids, dried from BNNT/CSA solution (see Experimental Section) to determine whether the BNNTs were irreversibly functionalized upon exposure to CSA. Sharp σ^* and π^* peaks arising from the B−K edge and a weak energy loss peak from the N−K edge at 188 and 401 eV, respectively, are characteristic of the electronic structure of hexagonal boron nitride, with boron and nitrogen having sp^2 hybridization.[51] This is consistent with a previous electron diffraction study by Smith et al., which indicated that the HTP BNNT material has a hexagonal crystal structure, with basal planes parallel to the tube surface.[45] Presence of an O−K edge loss peak in the EELS spectra of h-BN may originate from acid residues, the surrounding atmosphere, or possibly from reactor contamination. Since oxygen tends to adsorb chemically or physically on more defective areas, we observe it on h-BN structures with exposed edges, rather than on the BNNT surface.

Dissolving BNNTs in CSA without damage for direct observation of individual BNNTs by cryo-TEM opens a new approach for experimental characterization of the relative purity and structural damage. The following sections discuss in detail the characterization of BNNT solutions in CSA by cryo-TEM.

BNNT Defects. By cryo-TEM, we observe spontaneous filling of BNNTs with CSA, similarly to previous observations with CNTs.[42] Figure 3a shows both filled (black arrow) and empty (white arrow) BNNTs with significant contrast differences. The centers of empty BNNTs are much lighter than the surrounding acid matrix, because heavier sulfur and chlorine atoms in the CSA scatter electrons much more effectively than the lighter boron and nitrogen atoms. Conversely, filled BNNTs show little contrast relative to the background. Most of the imaged BNNTs are filled, implying the presence of defects along the walls, or open ends. A close-up view of a damaged end is shown in Figure 3b.

We find no correlation between BNNT diameter and the filling effect (within 3.5 to 5 nm range of diameters in the sample). Our images show that acid fills a BNNT whenever an open end or a damaged wall is present. As such, cryo-TEM imaging of BNNTs in CSA provides coarse material quality control for individual BNNTs. It is well-known that the presence of defects in nanometer-sized structures modifies their electronic and mechanical properties. Particularly, in the case of BNNTs, structural defects alter the band gap and chemical stability.[52,53] Figure 4a displays some clearly observed damaged

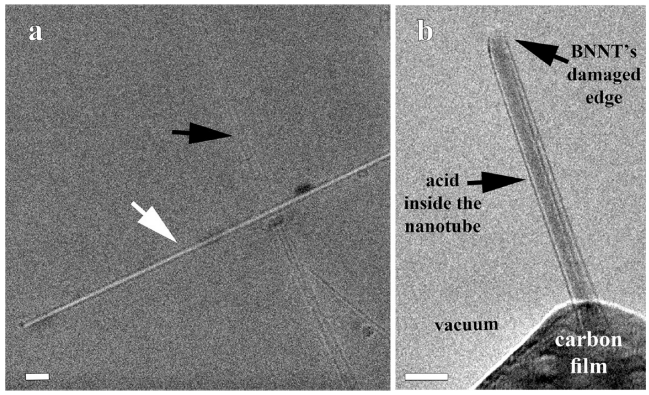

Figure 3. Cryo-TEM images, showing spontaneous filling. (a) Empty (white arrow) and filled (black arrow) BNNTs. (b) Damaged end of BNNT emerging from the vitrified acid. The opened end allows CSA to enter the tube. Scale bars = 20 nm.

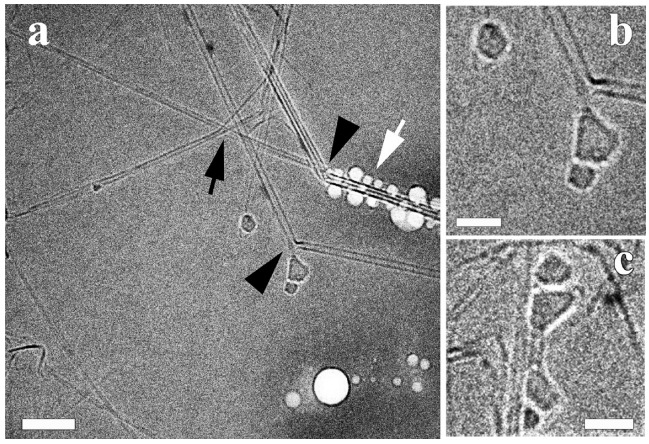

Figure 4. Cryo-TEM images of deformed and damaged BNNTs. (a) Black arrow points to a partially unzipped BNNT; black arrowheads show visible damage in the BNNT bent wall; white arrow points to electron beam damage at the CSA/BNNT interface. Scale bar = 50 nm. (b, c) Faceted structures in the studied BNNT batches. Scale bars = 20 nm.

BNNTs, e.g., partially unzipped (black arrow), bent (black arrowhead), and open BNNTs filled with acid. Although previous reports indicate Lewis bases at elevated temperature damage BNNTs through unzipping,[54,55] there is no indication that Brønsted acids at room temperature with no additional treatment would similarly damage BNNTs. In fact, the previously discussed EELS analysis of BNNT on TEM grids after coagulation and drying from BNNT/CSA solution eliminates the possibility that CSA damages the BNNTs. This finding is consistent with the high chemical resistance of BNNTs, with oxidation and cleavage known to occur only when sufficient energy is provided via high temperatures exceeding 700 °C,[56] plasma,[57] or ultrasonication.[58]

DOI: 10.1021/acs.langmuir.7b03461
Langmuir 2017, 33, 14340−14346

Interestingly, most bent BNNTs are characterized by v-shaped kinks, which can be explained by the tendency of BN structures to reduce the number of unfavorable B−B and N−N bonds at the sharp corners in the bending regions by formation of only polyhedrons with an even number of facets.[2,59] The studied BNNTs tend to form obtuse kink angles, ranging from 110° to 160° (based on statistics of 67 nanotubes imaged by cryo-TEM). Thicker BNNTs (more than 4.5 nm in diameter) undergo irreversible structural deformation at angles smaller than 126 ± 6° (Figure 4b). Several thinner BNNTs exhibit kink angles close to 90° (Figure 4c), while very short and thin BNNTs may have smooth kinks, rather than v-shaped ones. The correlation between number of facets of a polyhedron and kink angles may not be easily predicted or measured, since it varies with the diameter of the tube and synthesis condition. It is difficult to understand the reason for the deformation based on cryo-TEM images alone. However, taking into account the strong boron-to-nitrogen bonds, we hypothesize that structural defects involving atom displacement or vacancies are most likely caused by high local stress during BNNT synthesis. Note the faceted nanostructures, several nanometers in size, seen in the solution (Figure 4b,c). These nanostructures have sharp corners, are stable under the e-beam, and may either be a synthesis byproduct, or could have been formed by fracturing defective h-BN. Similar triangular structures were observed after h-BN monolayers were exposed to electrons at acceleration voltages of 80−200 kV in the HR-TEM.[60]

BNNT Synthesis Byproducts. Along with individual BNNTs dissolved in superacid, several features other than BNNTs were captured by direct cryo-TEM (Figure 5). We observed boron nitride (BN) clusters with nanotube-like edges (Figure 5a), unfolded BNNTs (Figure 5b), multilayered nanosheets with hexagonal facets (Figure 5c), and amorphous material on BNNT walls (Figure 5d). These impurities appeared in large quantities along with the desired HTP product, BNNTs.

Some BNNTs have angular ends (Figure 5a). Hemispherical ends are energetically unfavorable because they require odd numbered rings that, in turn, require N−N or B−B bonds.[61] The unfolded conical edge of a BNNT observed in Figure 5b supports the notion of nanoribbon formation from BNNTs[57] and theoretical calculations of energetically preferable tapered edges for BNNTs.[62,63] Multilayered hexagonal sheets are also captured by cryo-TEM (Figure 5c), while some BNNTs are covered by amorphous material (Figure 5d). All mentioned structures were also observed by HR-SEM analysis of HTP BNNTs prior to mixing with CSA (Figure 6), supporting the notion that non-nanotubes are synthesis byproducts.

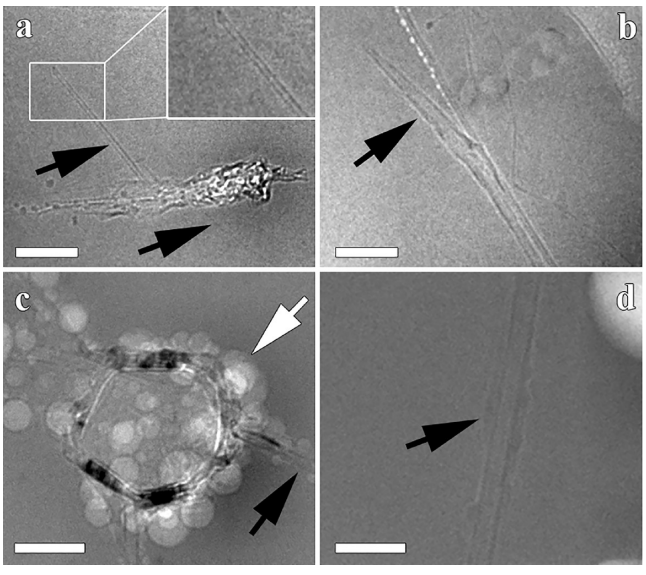

Figure 5. Cryo-TEM micrographs of nanostructures present in the BNNT/CSA solution. (a) Boron nitride cluster, left over during BNNT synthesis, together with individual BNNTs (arrows). Inset: BNNT angular edge, typical of studied BNNTs. (b) Unfolded BNNT end (arrow). (c) Multilayered hexagonal sheets. Bright cavities are e-beam radiation damage at the nanosheet/CSA interface (white arrow). Note BNNTs in the background (black arrow). (d) Amorphous material covering the BNNTs (arrow). Scale bars: (a, b) = 100 nm, (c, d) = 50 nm.

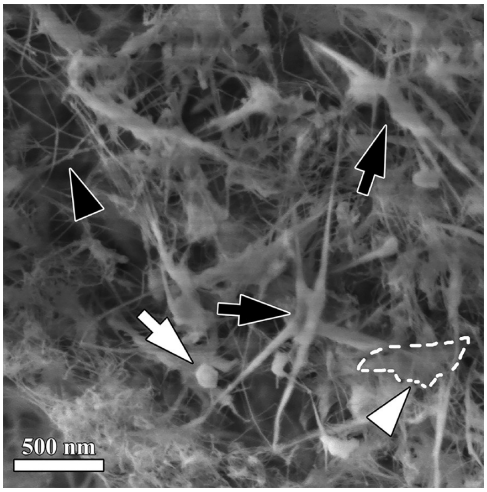

Figure 6. HR-SEM micrograph of BNNTs before dissolution in CSA. Black arrows, boron nitride clusters; white arrow, boron nitride hexagonal particles encapsulating boron; white arrowhead, multilayer boron nitride sheet (outlined); black arrowhead, BNNTs.

Elemental map images created with energy-filtered transmission electron microscopy (EFTEM) confirms that the nanotubes are BN (white arrowhead in Figure 7). On filtered images for boron and nitrogen (Figure 7, right), the BNNTs exhibit medium brightness levels in both maps, consistent with the expected B and N content.

Besides BNNTs, small nanometric structures similar in size to the BNNT diameter were frequently observed in the BNNT product in cryo-TEM and HRSEM modes. These were identified as unreacted boron particles encapsulated by thin layers of crystalline BN (arrows in Figure 7). These nanoparticles appear with bright cores in the B map and bright edges in the N map, indicating solid boron cores with BN growth on the surface. The B map of bigger hexagonal structures shows intense signal from the entire particle, while the N map exhibits strong signal from the particle edges only. This indicates h-BN layer overlapping a boron rich layer. The most probable scenario is that multilayered h-BN tends to grow on the surface of boron clusters or big particles, because partially dissolved nitrogen on the molten boron surface can readily form BN layers when cooling. The formation of flat faceted h-BN layers on curved surfaces, such as tube ends or spheres, agrees with previous observations[3] and a computational model developed by Yamakov et al.,[64] which indicates that faceting releases the strain energy of mismatched B−N

DOI: 10.1021/acs.langmuir.7b03461
Langmuir 2017, 33, 14340−14346

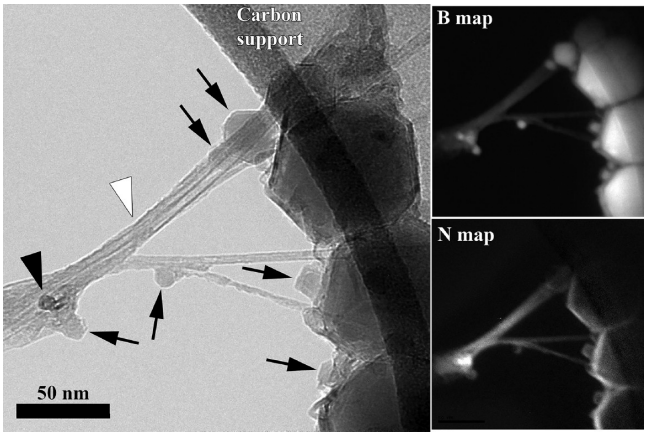

Figure 7. EFTEM mapping of BNNTs and related microstructures. Left micrograph: bright field TEM mode, a zero loss image. The maps on the right are boron and nitrogen elemental maps in the STEM mode. There is a correlation between observed structures and elemental mapping: The white arrowhead points to a BNNT pair. When an end of one of the BNNTs turns parallel to the e-beam (black arrowhead), boron and nitrogen counts from the end are enhanced. Boron particles 10−30 nm in size are marked with arrows, while bigger hexagonal structures are related to B-rich layers, covered by h-BN layers. Nitrogen and boron signals from h-BN structures are shielded by the carbon support.

bonds between adjacent layers. The structural deformation of h-BN also explains why those structures tend to adsorb oxygen more readily than BNNTs (see EELS analysis).

The presence of significant quantities of unwanted nanomaterials detected in the BNNT batch indicates that uncontrolled arrangement of the boron and nitrogen sources reduces the BNNT yield. Even with a true solvent for BNNTs, processing may still be limited by the presence of impurities. Therefore, optimization of reactor conditions is important for production of pure BNNTs as the major product. Because of the current lack of efficient purification techniques, the identification and classification of non-BNNT material in the synthesis product is essential for controlled, high-quality BNNT synthesis, and for the development of postprocessing purification methods.

SUMMARY AND CONCLUSIONS

In this study, we characterized BNNTs produced by the HTP method. We characterized BNNT structure and morphology after dissolution in CSA. By cryo-TEM, we demonstrated for the first time the dissolution of BNNTs in CSA at the molecular level. Separation of BNNTs into individual molecules is a promising step toward their transforming into macroscopic scalable products, such as fibers and films. In addition, the current study suggests a characterization route of nanomaterials dissolved in superacid with extensive use of electron microscopy. We determined the BNNT length, presence of defects, and other "synthesis fingerprints," such as impurities and synthesis byproducts. We found micrometer-long, predominantly double-walled BNNTs with average diameter of 3.8 ± 0.2 nm, along with non-nanotube BN nanometric structures, such as single- and multilayer h-BN, amorphous material on tube walls, and BN clusters. Defective and bent BNNTs present in CSA solutions were imaged by cryo-TEM. The abundance of impurities dramatically limits the quality of BNNTs acid solutions, whereas structural defects degrade the BNNT intrinsic properties. Analysis of the HTP BNNTs before and after mixing with CSA by several microscopic techniques indicated reversible BNNT dissolution in CSA, without damaging or chemically modifying the BNNT, and revealed sp^2 hybridization of BN studied nanospecies. Accurate characterization of unwanted material in the BNNT batches have critical importance for optimization of BNNT synthesis to increase BNNT yield and for the development of efficient BNNT purification methods.

ASSOCIATED CONTENT

Supporting Information

The Supporting Information is available free of charge on the ACS Publications website at DOI: 10.1021/acs.langmuir.7b03461.

HR-TEM micrographs of BNNT, statistical diameter and length measurements details, and EELS analysis spectra and corresponding images (PDF)

AUTHOR INFORMATION

Corresponding Authors

*E-mail: mp@rice.edu.
*E-mail: ishi@technion.ac.il.

ORCID

Olga Kleinerman: 0000-0001-7139-0999
Matteo Pasquali: 0000-0001-5951-395X
Yeshayahu Talmon: 0000-0002-9854-3972

Present Address

⊥A.W.K.M.: Department of Chemical and Biomolecular Engineering and Institute of Materials Science, University of Connecticut, Storrs, CT 06269, USA.

Funding

M.A. acknowledges the financial support through the Ph.D. scholarship from Abu Dhabi National Oil Company (ADNOC). D.M. was partially supported by a Wiess teacher-scholar fellowship. Funding was provided by AFOSR grants FA9550-15-1-0370, FA9550-09-1-0590, the Robert A. Welch Foundation (C-1668), NASA grant NNX15AK72G, NSF grant CHE-1610175, and the United States-Israel Binational Science Foundation.

Notes

The authors declare no competing financial interest.

ACKNOWLEDGMENTS

We are grateful to Dr. Yaron Kauffmann for his help with the STEM and EELS analysis, performed at the Technion Electron Microscopy Center at the Department of Materials Science & Engineering (Haifa, Israel), and to Roy Crooks (Black Laboratories, LLC, Newport News VA 23601) for his assistance with EFTEM data acquisition. Cryo-TEM and HR-SEM were performed at the Center for Electron Microscopy of Soft Matter, supported by the Technion Russell Berrie Nanotechnology Institute (RBNI) (Haifa, Israel). Elemental maps were acquired at NASA Langley Research Center, Advanced Materials and Processing Branch (Hampton VA 23681).

REFERENCES

(1) Chopra, N. G.; Luyken, R. J.; Cherrey, K.; Crespi, V. H.; Cohen, M. L.; Louie, S. G.; Zettl, A. Boron Nitride Nanotubes. *Science (Washington, DC, U. S.)* **1995**, *269* (5226), 966−967.

DOI: 10.1021/acs.langmuir.7b03461
Langmuir 2017, 33, 14340−14346

(2) Ghassemi, H. M.; Lee, C. H.; Yap, Y. K.; Yassar, R. S. Real-Time Fracture Detection of Individual Boron Nitride Nanotubes in Severe Cyclic Deformation Processes. *J. Appl. Phys.* **2010**, *108* (2), 024314.
(3) Golberg, D.; Bando, Y.; Huang, Y.; Terao, T.; Mitome, M.; Tang, C.; Zhi, C. Boron Nitride Nanotubes and Nanosheets. *ACS Nano* **2010**, *4* (6), 2979−2993.
(4) Terrones, M.; Romo-Herrera, J. M.; Cruz-Silva, E.; López-Urías, F.; Muñoz-Sandoval, E.; Velázquez-Salazar, J. J.; Terrones, H.; Bando, Y.; Golberg, D. Pure and Doped Boron Nitride Nanotubes. *Mater. Today* **2007**, *10* (5), 30−38.
(5) Vaccarini, L.; Goze, C.; Henrard, L.; Hernández, E.; Bernier, P.; Rubio, A. Mechanical and Electronic Properties of Carbon and Boron−nitride Nanotubes. *Carbon* **2000**, *38* (11−12), 1681−1690.
(6) Verma, V.; Jindal, V. K.; Dharamvir, K. Elastic Moduli of a Boron Nitride Nanotube. *Nanotechnology* **2007**, *18* (43), 435711.
(7) Chen, Y.; Zou, J.; Campbell, S. J.; Le Caer, G. Le. Boron Nitride Nanotubes: Pronounced Resistance to Oxidation. *Appl. Phys. Lett.* **2004**, *84* (13), 2430−2432.
(8) Chang, C. W.; Fennimore, A. M.; Afanasiev, A.; Okawa, D.; Ikuno, T.; Garcia, H.; Li, D.; Majumdar, A.; Zettl, A. Isotope Effect on the Thermal Conductivity of Boron Nitride Nanotubes. *Phys. Rev. Lett.* **2006**, *97* (8), 85901.
(9) Rubio, A.; Corkill, J. L.; Cohen, M. L. Theory of Graphitic Boron Nitride Nanotubes. *Phys. Rev. B: Condens. Matter Mater. Phys.* **1994**, *49* (7), 5081−5084.
(10) Zhi, C.; Bando, Y.; Tang, C.; Golberg, D. Boron Nitride Nanotubes. *Mater. Sci. Eng., R* **2010**, *70* (3−6), 92−111.
(11) Zhi, C.; Bando, Y.; Tang, C.; Golberg, D.; Xie, R.; Sekigushi, T. Phonon Characteristics and Cathodolumininescence of Boron Nitride Nanotubes. *Appl. Phys. Lett.* **2005**, *86* (21), 213110.
(12) Chang, C. W.; Okawa, D.; Garcia, H.; Majumdar, A.; Zettl, A. Nanotube Phonon Waveguide. *Phys. Rev. Lett.* **2007**, *99* (4), 45901.
(13) Kang, J. H.; Sauti, G.; Park, C.; Yamakov, V. I.; Wise, K. E.; Lowther, S. E.; Fay, C. C.; Thibeault, S. A.; Bryant, R. G. Multifunctional Electroactive Nanocomposites Based on Piezoelectric Boron Nitride Nanotubes. *ACS Nano* **2015**, *9* (12), 11942−11950.
(14) Yamakov, V.; Park, C.; Kang, J. H.; Chen, X.; Ke, C.; Fay, C. Piezoelectric and Elastic Properties of Multiwall Boron-Nitride Nanotubes and Their Fibers: A Molecular Dynamics Study. *Comput. Mater. Sci.* **2017**, *135*, 29−42.
(15) Thibeault, S. A.; Kang, J. H.; Sauti, G.; Park, C.; Fay, C. C.; King, G. C. Nanomaterials for Radiation Shielding. *MRS Bull.* **2015**, *40* (10), 836−841.
(16) Ganji, M. D.; Mirnejad, A.; Najafi, A. Theoretical Investigation of Methane Adsorption onto Boron Nitride and Carbon Nanotubes. *Sci. Technol. Adv. Mater.* **2010**, *11* (4), 045001.
(17) Lim, S. H.; Luo, J.; Ji, W.; Lin, J. Synthesis of Boron Nitride Nanotubes and Its Hydrogen Uptake. *Catal. Today* **2007**, *120* (3−4), 346−350.
(18) Mpourmpakis, G.; Froudakis, G. E. Why Boron Nitride Nanotubes Are Preferable to Carbon Nanotubes for Hydrogen Storage?: An Ab Initio Theoretical Study. *Catal. Today* **2007**, *120* (3−4), 341−345.
(19) Shadman, M.; Ahadi, Z. Argon and Neon Storages in Single-Walled Boron Nitride Nanotubes: A Grand Canonical Monte-Carlo Study. *Fullerenes, Nanotubes, Carbon Nanostruct.* **2011**, *19* (8), 700−712.
(20) Enyashin, A. N.; Ivanovskii, A. L. Deformation Mechanisms for Carbon and Boron Nitride Nanotubes. *Inorg. Mater.* **2006**, *42* (12), 1336−1341.
(21) Golberg, D.; Costa, P. M. F. J.; Wang, M. S.; Wei, X.; Tang, D. M.; Xu, Z.; Huang, Y.; Gautam, U. K.; Liu, B.; Zeng, H.; et al. Nanomaterial Engineering and Property Studies in a Transmission Electron Microscope. *Adv. Mater.* **2012**, *24* (2), 177−194.
(22) Ju, S.-P.; Wang, Y.-C.; Lien, T.-W. Tuning the Electronic Properties of Boron Nitride Nanotube by Mechanical Uni-Axial Deformation: A DFT Study. *Nanoscale Res. Lett.* **2011**, *6* (1), 160−171.
(23) Bai, X.; Golberg, D.; Bando, Y.; Zhi, C.; Tang, C.; Mitome, M.; Kurashima, K. Deformation-Driven Electrical Transport of Individual Boron Nitride Nanotubes. *Nano Lett.* **2007**, *7* (3), 632−637.
(24) Khoo, K. H.; Mazzoni, M. S. C.; Louie, S. G. Tuning the Electronic Properties of Boron Nitride Nanotubes with Transverse Electric Fields: A Giant Dc Stark Effect. *Phys. Rev. B: Condens. Matter Mater. Phys.* **2004**, *69* (20), 201401.
(25) Zhi, C. Y.; Bando, Y.; Tang, C. C.; Huang, Q.; Golberg, D. Boron Nitride Nanotubes: Functionalization and Composites. *J. Mater. Chem.* **2008**, *18*, 3900−3908.
(26) Terao, T.; Zhi, C.; Bando, Y.; Mitome, M.; Tang, C.; Golberg, D. Alignment of Boron Nitride Nanotubes in Polymeric Composite Films for Thermal Conductivity Improvement. *J. Phys. Chem. C* **2010**, *114* (10), 4340−4344.
(27) Li, L.; Chen, Y.; Stachurski, Z. H. Boron Nitride Nanotube Reinforced Polyurethane Composites. *Prog. Nat. Sci.* **2013**, *23* (2), 170−173.
(28) Jakubinek, M. B.; Niven, J. F.; Johnson, M. B.; Ashrafi, B.; Kim, K. S.; Simard, B.; White, M. A. Thermal Conductivity of Bulk Boron Nitride Nanotube Sheets and Their Epoxy-Impregnated Composites. Phys. *Phys. Status Solidi A* **2016**, *213* (8), 2237−2242.
(29) Kim, K. S.; Kim, M. J.; Park, C.; Fay, C. C.; Chu, S.-H.; Kingston, C. T.; Simard, B. Scalable Manufacturing of Boron Nitride Nanotubes and Their Assemblies: A Review. *Semicond. Sci. Technol.* **2017**, *32* (1), 013003.
(30) Ikuno, T.; Sainsbury, T.; Okawa, D.; Fréchet, J. M. J.; Zettl, A. Amine-Functionalized Boron Nitride Nanotubes. *Solid State Commun.* **2007**, *142* (11), 643−646.
(31) Yu, J.; Chen, Y.; Cheng, B. M. Dispersion of Boron Nitride Nanotubes in Aqueous Solution with the Help of Ionic Surfactants. *Solid State Commun.* **2009**, *149* (19−20), 763−766.
(32) Gao, Z.; Zhi, C.; Bando, Y.; Golberg, D.; Serizawa, T. Isolation of Individual Boron Nitride Nanotubes via Peptide Wrapping. *J. Am. Chem. Soc.* **2010**, *132* (14), 4976−4977.
(33) Velayudham, S.; Lee, C. H.; Xie, M.; Blair, D.; Bauman, N.; Yap, Y. K.; Green, S. A.; Liu, H. Noncovalent Functionalization of Boron Nitride Nanotubes with Poly(p-Phenylene-Ethynylene)s and Poly-thiophene. *ACS Appl. Mater. Interfaces* **2010**, *2* (1), 104−110.
(34) Zhang, Z. W.; Zheng, W. T.; Jiang, Q. Hydrogen Adsorption on Ce/BNNT Systems: A DFT Study. *Int. J. Hydrogen Energy* **2012**, *37* (6), 5090−5099.
(35) Kim, D.; Sawada, T.; Zhi, C.; Bando, Y.; Golberg, D.; Serizawa, T. Dispersion of Boron Nitride Nanotubes in Aqueous Solution by Simple Aromatic Molecules. *J. Nanosci. Nanotechnol.* **2014**, *14* (4), 3028−3033.
(36) Zeng, X. J.; Liu, W. L. Dispersion of Boron Nitride Nanotubes in Non-Aqueous Solution. *Micro Nano Lett.* **2014**, *9* (9), 569−571.
(37) Shin, H.; Guan, J.; Zgierski, M. Z.; Kim, K. S.; Kingston, C. T.; Simard, B. Covalent Functionalization of Boron Nitride Nanotubes via Reduction Chemistry. *ACS Nano* **2015**, *9* (12), 12573−12582.
(38) Tiano, A. L.; Gibbons, L.; Tsui, M.; Applin, S. I.; Silva, R.; Park, C.; Fay, C. C. Thermodynamic Approach to Boron Nitride Nanotube Solubility and Dispersion. *Nanoscale* **2016**, *8* (7), 4348−4359.
(39) Ramesh, S.; Ericson, L. M.; Davis, V. A.; Saini, R. K.; Kittrell, C.; Pasquali, M.; Billups, W. E.; Adams, W. W.; Hauge, R. H.; Smalley, R. E. Dissolution of Pristine Single Walled Carbon Nanotubes in Superacids by Direct Protonation. *J. Phys. Chem. B* **2004**, *108* (26), 8794−8798.
(40) Davis, V. A.; Parra-Vasquez, A. N. G.; Green, M. J.; Rai, P. K.; Behabtu, N.; Prieto, V.; Booker, R. D.; Schmidt, J.; Kesselman, E.; Zhou, W.; et al. True Solutions of Single-Walled Carbon Nanotubes for Assembly into Macroscopic Materials. *Nat. Nanotechnol.* **2009**, *4* (12), 830−834.
(41) Duque, J. G.; Parra-Vasquez, A. N. G.; Behabtu, N.; Green, M. J.; Higginbotham, A. L.; Price, B. K.; Leonard, A. D.; Schmidt, H. K.; Lounis, B.; Tour, J. M.; et al. Diameter-Dependent Solubility of Single-Walled Carbon Nanotubes. *ACS Nano* **2010**, *4* (6), 3063−3072.
(42) Green, M. J.; Young, C. C.; Parra-Vasquez, A. N. G.; Majumder, M.; Juloori, V.; Behabtu, N.; Pint, C. L.; Schmidt, J.; Kesselman, E.;

DOI: 10.1021/acs.langmuir.7b03461
Langmuir 2017, 33, 14340−14346

Hauge, R. H.; et al. Direct Imaging of Carbon Nanotubes Spontaneously Filled with Solvent. *Chem. Commun.* **2011**, *47* (4), 1228−1230.
(43) Kleinerman, O.; Parra-Vasquez, A. N. G.; Green, M. J.; Behabtu, N.; Schmidt, J.; Kesselman, E.; Young, C. C.; Cohen, Y.; Pasquali, M.; Talmon, Y. Cryogenic-Temperature Electron Microscopy Direct Imaging of Carbon Nanotubes and Graphene Solutions in Superacids. *J. Microsc.* **2015**, *259* (1), 16−25.
(44) Jasuja, K. Designing Nanoscale Constructs from Atomic Thin Sheets of Graphene, Boron Nitride and Gold Nanoparticles for Advanced Material Applications. Ph.D. Thesis, Kansas State University, 2011.
(45) Smith, M. W.; Jordan, K. C.; Park, C.; Kim, J.-W.; Lillehei, P. T.; Crooks, R.; Harrison, J. S. Very Long Single- and Few-Walled Boron Nitride Nanotubes via the Pressurized Vapor/condenser Method. *Nanotechnology* **2009**, *20* (50), 505604.
(46) Kleinerman, O.; Liberman, L.; Behabtu, N.; Pasquali, M.; Cohen, Y.; Talmon, Y. Direct Imaging of Carbon Nanotube Liquid-Crystalline Phase Development in True Solutions. *Langmuir* **2017**, *33* (16), 4011−4018.
(47) Bellare, J. R.; Davis, H. T.; Scriven, L. E.; Talmon, Y. Controlled Environment Vitrification System: An Improved Sample Preparation Technique. *J. Electron Microsc. Tech.* **1988**, *10* (1), 87−111.
(48) Siegel, D. P.; Green, W. J.; Talmon, Y. The Mechanism of Lamellar-to-Inverted Hexagonal Phase Transitions: A Study Using Temperature-Jump Cryo-Electron Microscopy. *Biophys. J.* **1994**, *66* (2 Pt 1), 402−414.
(49) Bengio, E. A.; Tsentalovich, D. E.; Behabtu, N.; Kleinerman, O.; Kesselman, E.; Schmidt, J.; Talmon, Y.; Pasquali, M. Statistical Length Measurement Method by Direct Imaging of Carbon Nanotubes. *ACS Appl. Mater. Interfaces* **2014**, *6* (9), 6139−6146.
(50) Park, C.; Crooks, R. E.; Siochi, E. J.; Harrison, J. S.; Evans, N.; Kenik, E. Adhesion Study of Polyimide to Single-Wall Carbon Nanotube Bundles by Energy-Filtered Transmission Electron Microscopy. *Nanotechnology* **2003**, *14* (9), L11.
(51) Huang, J. Y.; Jia, X. B.; Yasuda, H.; Mori, H. Stacking Disordering in Hexagonal BN Induced by Shearing under Ball Milling. *Philos. Mag. Lett.* **1999**, *79* (5), 217−224.
(52) Kang, H. S. Theoretical Study of Boron Nitride Nanotubes with Defects in Nitrogen-Rich Synthesis. *J. Phys. Chem. B* **2006**, *110* (10), 4621−4628.
(53) Matarín, O.; Rimola, A. Influence of Defects in Boron Nitride Nanotubes in the Adsorption of Molecules. Insights from B3LYP-D2* Periodic Simulations. *Crystals* **2016**, *6* (5), 63.
(54) Pal, S.; Vivekchand, S. R. C.; Govindaraj, A.; Rao, C. N. R. Functionalization and Solubilization of BN Nanotubes by Interaction with Lewis Bases. *J. Mater. Chem.* **2007**, *17* (5), 450−452.
(55) Liao, Y.; Chen, Z.; Connell, J. W.; Fay, C. C.; Park, C.; Kim, J.-W.; Lin, Y. Chemical Sharpening, Shortening, and Unzipping of Boron Nitride Nanotubes. *Adv. Funct. Mater.* **2014**, *24* (28), 4497−4506.
(56) Nautiyal, P.; Loganathan, A.; Agrawal, R.; Boesl, B.; Wang, C.; Agarwal, A. Oxidative Unzipping and Transformation of High Aspect Ratio Boron Nitride Nanotubes into "White Graphene Oxide" Platelets. *Sci. Rep.* **2016**, *6* (1), 29498.
(57) Zeng, H.; Zhi, C.; Zhang, Z.; Wei, X.; Wang, X.; Guo, W.; Bando, Y.; Golberg, D. "White Graphenes": Boron Nitride Nanoribbons via Boron Nitride Nanotube Unwrapping. *Nano Lett.* **2010**, *10* (12), 5049−5055.
(58) Lee, C. H.; Zhang, D.; Yap, Y. K. Functionalization, Dispersion, and Cutting of Boron Nitride Nanotubes in Water. *J. Phys. Chem. C* **2012**, *116*, 1798−1804.
(59) Ghassemi, H. M.; Lee, C. H.; Yap, Y. K.; Yassar, R. S. Situ Observation of Reversible Rippling in Multi-Walled Boron Nitride Nanotubes. *Nanotechnology* **2011**, *22* (11), 115702−115707.
(60) Kotakoski, J.; Jin, C. H.; Lehtinen, O.; Suenaga, K.; Krasheninnikov, A. V. Electron Knock-on Damage in Hexagonal Boron Nitride Monolayers. *Phys. Rev. B: Condens. Matter Mater. Phys.* **2010**, *82* (11), 1−4.
(61) Altoe, M. V. P.; Sprunck, J. P.; Gabriel, J.-C.; Bradley, P. K. Nanococoon Seeds for BN Nanotube Growth. *J. Mater. Sci.* **2003**, *38* (24), 4805−4810.
(62) Bourgeois, L.; Bando, Y.; Han, W. Q.; Sato, T. Structure of Boron Nitride Nanoscale Cones: Ordered Stacking of 240° and 300° Disclinations. *Phys. Rev. B: Condens. Matter Mater. Phys.* **2000**, *61* (11), 7686−7691.
(63) Han, W. Q.; Bourgeois, L.; Bando, Y.; Kurashima, K.; Sato, T. Formation and Structure of Boron Nitride Conical Nanotubes. *Appl. Phys. A: Mater. Sci. Process.* **2000**, *71* (1), 83−85.
(64) Yamakov, V.; Park, C.; Kang, J. H.; Chen, X.; Ke, C.; Fay, C. Piezoelectric and Elastic Properties of Multiwall Boron-Nitride Nanotubes and Their Fibers: A Molecular Dynamics Study. *Comput. Mater. Sci.* **2017**, *135*, 29−42.

DOI: 10.1021/acs.langmuir.7b03461
Langmuir 2017, 33, 14340−14346